Biosensors and Bioelectronics 24 (2008) 383–390

Contents lists available at ScienceDirect

Biosensors and Bioelectronics

journal homepage: www.elsevier.com/locate/bios

Time-resolved Förster-resonance-energy-transfer DNA assay on an active CMOS microarray

David Eric Schwartz*, Ping Gong, Kenneth L. Shepard

Bioelectronic Systems Laboratory, Department of Electrical Engineering, Columbia University, 1300 S.W. Mudd Building, 500 West 120th Street, NY, 10027, USA

ARTICLE INFO

Article history:
Received 7 March 2008
Received in revised form 15 April 2008
Accepted 17 April 2008
Available online 26 April 2008

Keywords:
Oligonucleotide microarray
Active microarray
Single-photon avalanche diode
SPAD array
TR-FRET
Quantum dots

ABSTRACT

We present an active oligonucleotide microarray platform for time-resolved Förster-resonance-energy-transfer (TR-FRET) assays. In these assays, immobilized probe is labeled with a donor fluorophore and analyte target is labeled with a fluorescence quencher. Changes in the fluorescence decay lifetime of the donor are measured to determine the extent of hybridization. In this work, we demonstrate that TR-FRET assays have reduced sensitivity to variances in probe surface density compared with standard fluorescence-based microarray assays. Use of an active array substrate, fabricated in a standard complementary metal-oxide-semiconductor (CMOS) process, provides the additional benefits of reduced system complexity and cost. The array consists of 4096 independent single-photon avalanche diode (SPAD) pixel sites and features on-chip time-to-digital conversion. We demonstrate the functionality of our system by measuring a DNA target concentration series using TR-FRET with semiconductor quantum dot donors.

1. Introduction

DNA microarrays have risen to prominence in genomics with a breadth of applications ranging from polymorphism and mutation detection (Peeters and Van der Spek, 2005) to forensic analysis (Divne and Allen, 2005). In epidemiology, they have been used to identify pathogens (Wilson et al., 2002), to characterize benzene poisoning (Forrest et al., 2005), and for genotyping virus strains (Song et al., 2006). They can be used to evaluate the progression of many diseases, including leukemia (Schroers et al., 2005) and ovarian cancer (Motamed-Khorasani et al., 2007). They are also a valuable tool in pharmacogenetics, for example, to screen chemotherapy drugs for efficacy and toxicity (Watters and McLeod, 2003) and for psychotropic drug development (Murphy, 2006).

In many regards, microarray technology has matured greatly since its introduction (Hoheisel, 2006). Current technologies allow up to one-million-site multiplexing and accurate single nucleotide polymorphism (SNP) detection (Chittur, 2004). Probe spot diameters are as small as 11 μm (Kawasaki, 2006). These achievements have been made possible through vast improvements in parallelism, throughput, and sensitivity resulting from advances in probe design, surface chemistry, probe deposition techniques, and statistical data analysis (Heller, 2002). Nevertheless, challenges remain with current microarray technologies.

One persistent issue is spot variability (Draghici et al., 2006), primarily determined by variance in probe immobilization (Auburn et al., 2005), which is affected by spotting time, temperature, humidity, spotting and hybridization solution composition, and inconsistencies in the microarray substrate surface itself (Mary-Huard et al., 2004). Replication is generally employed to enable statistical averaging of this variability but this reduces throughput (Ramakrishnan et al., 2002), and quantitative analysis is still restricted to relative rather than absolute concentrations of analyte (Hoheisel, 2006).

At the same time, the basic techniques of immobilizing probe on a passive glass substrate, hybridizing with fluorophore-labeled-target, and imaging in a laboratory-scale microarray scanner have remained fundamentally the same. This limits microarray applications to research environments due to the size and expense of detection hardware (Heller, 2002).

In a standard oligonucleotide microarray expression assay, known DNA probe sequences are bound to sites on a functionalized substrate and exposed to target analyte molecules modified with fluorescent labels. The microarray is then illuminated and the relative intensity of the fluorophore emission at each site is measured. This emission intensity is correlated to the quantity of bound target at each site and can be used to estimate the relative concentrations

* Corresponding author. Tel.: +1 212 854 0398.
E-mail address: des@cisl.columbia.edu (D.E. Schwartz).

0956-5663/$ – see front matter © 2008 Elsevier B.V. All rights reserved.
doi:10.1016/j.bios.2008.04.015

of target molecules complementary to each probe sequence (Heller, 2002).

A donor-only time-resolved Förster-resonance-energy-transfer (TR-FRET) oligonucleotide microarray assay differs from a conventional assay in that the fluorescent label is attached to the immobilized probe instead of the analyte target and its lifetime, rather than its intensity, is measured. To perform the assay, a "donor" fluorophore is attached to one end of an immobilized DNA probe molecule and a compatible fluorescence quencher is attached to the complementary end of each target molecule. Upon hybridization, a FRET interaction between the donor and quencher is induced, leading to a reduction in the donor fluorescence lifetime. The change in average donor lifetime can be used to determine the complementary target concentration for each probe sequence (Cardullo et al., 1988).

Whereas in a standard assay the signal is dependent on the number of bound target molecules, the signal in a TR-FRET assay is determined by the fraction of probe molecules associated with bound target. This leads to reduced signal variability with probe surface coverage. In addition, in a TR-FRET assay, unbound target in the hybridization solution does not affect the signal, obviating the need for rinsing before measurement.

Time-resolved fluorescence detection approaches applicable to TR-FRET assays have been developed for fluorescence lifetime imaging microscopy (FLIM) applications. Time-domain FLIM systems employ pulsed laser sources to stimulate fluorophores and one of two approaches for the detection of the induced fluorescence.

In the first approach, either a charge-coupled device (CCD) or complementary metal-oxide-semiconductor (CMOS) photodiode-based imager is employed. Gating is usually effected by an intensifier which precedes the imager (Wang et al., 1991; Dowling et al., 1997; Nicholas and Barry, 2006). By comparing the intensity integrated over time windows with varying offsets, the fluorescence decay function can be calculated. Complex multiexponential decay functions require repeated measurements, increasing overall measurement times (Sharman et al., 1999; De Grauw and Gerristen, 2001).

The second detection approach in FLIM is time-correlated single-photon counting (TCSPC), implemented by repeatedly stimulating a fluorophore and recording the time until the first emitted photon is detected by a sensor. A histogram of the number of photons arriving per time bin is constructed and as long as the probability of photon detection for each measurement is sufficiently low (no greater than one photon per approximately one hundred measurements), the histogram will correlate with the intensity decay profile of the fluorophore (Harris and Selinger, 1979). A TCSPC system requires a high-gain sensor capable of single-photon detection, usually a photomultiplier tube (PMT), and a method of accurately measuring time intervals. PMTs employ high electric fields and secondary electron emission effects to generate picoampere currents from incident photons. They are bulky, expensive, and not easily formed into arrays. As a result, laser scanning is necessary, complicating the optical setup and leading to a measurement time that scales linearly with imaged area (Becker et al., 2004).

An alternative to the PMT is the single-photon avalanche diode (SPAD), a solid-state device that converts arriving photons into measurable current pulses through avalanche breakdown of a semiconductor junction. Recently, SPADs have been fabricated in standard CMOS technologies (Rochas et al., 2002) enabling active two-dimensional arrays integrated with time-to-digital conversion circuits, eliminating the need for laser scanning and greatly reducing the complexity and cost of detector systems.

In this paper, we present a demonstration system that utilizes a custom SPAD-based CMOS imager as an active substrate for a TR-FRET assay measuring hybridization through fluorescence lifetime changes. The active CMOS microarray substrate, in which probe is immobilized directly on or above an array of detectors, replaces the traditional confocal scanner, allowing for an integrated, portable detection platform that incorporates data conversion and data processing on chip. Because we have designed a custom chip for this application, our design differs from previous work (Lamture et al., 1994; Vo-Dinh et al., 1999; Mallard et al., 2005) in which conventional imager chips were employed as active platforms. The unique capabilities of this chip for time-gated, time-resolved measurement enable TR-FRET applications. On-chip TCSPC with SPADs also allows for higher sensitivities than traditional imagers based on integrating photocurrents. The use of TR-FRET allows for the direct quantification of the fraction of bound target, reducing susceptibility to probe coverage variation.

2. Experimental

2.1. The CMOS active microarray

We have developed a 64-by-64 array of active SPAD sensor "pixels" with on-chip time-to-digital conversion and supporting circuitry. The details of the chip are described in Schwartz et al. (2007). The array is capable both of TR-FRET measurement using TCSPC and standard intensity-based measurement, which can be accomplished by computing the average photon arrival probability in a fixed time window after stimulation of the fluorophore. Used as an active array platform, probes are spotted directly on or above the surface of the chip. To facilitate this, the chip is assembled in a ball-grid-array package and encapsulated with a combination of Hysol FP4450 and Hysol FP4451 epoxies (Henkel KGaA, Düsseldorf, Germany), protecting the bonding wires from hybridization buffers and other solutions while keeping the sensor array of the chip exposed. Photographs of the packaged array appear in Fig. 1A.

The array is fabricated in a commercial 0.35-μm CMOS process and measures 4 mm × 4 mm. The active area of each SPAD sensor is 15 μm^2 and the pixel pitch is 40 μm. Accurate timing is maintained with a delay-locked-loop-stabilized multiphase clock. Each of the 64 columns of the array has an individual time-to-digital converter (TDC) which latches the arrival-time information of photons within that column of the array. The TDCs have a timing resolution of 350 ps. The noise floor is determined by an average dark count rate of 1059 Hz, corresponding to approximately two to four photons per one thousand measurements.

2.2. Lifetime measurement technique

Fluorescence lifetimes are measured using our array synchronized to a PiLAS 406-nm gain-switched diode laser (Advanced Laser Diode Systems, Berlin, Germany) with a DG-535 delay generator (Stanford Research Systems, Sunnyvale, CA, USA) and triggered at 5 kHz. The laser pulse has a full duration at half maximum of approximately 36 ps, and the average pulse energy is 40 pJ, corresponding to 8.2×10^7 photons. The beam is focused onto an area of approximately 4 mm^2, giving a photon flux density of 2×10^9 photons cm^{-2}.

Fig. 1B shows a simplified diagram of the measurement setup. A sample of analyte, such as DNA, could be immobilized directly on the chip surface. Instead, to ease surface preparation, we immobilize the sample on a glass slide which is carefully scored and broken to fit within the donut epoxy surrounding the array (see Fig. 1A) and then inverted over the sensor site, bringing the sample into contact with the chip surface and minimizing optical losses. As the measurement is time-resolved and the laser impulse is

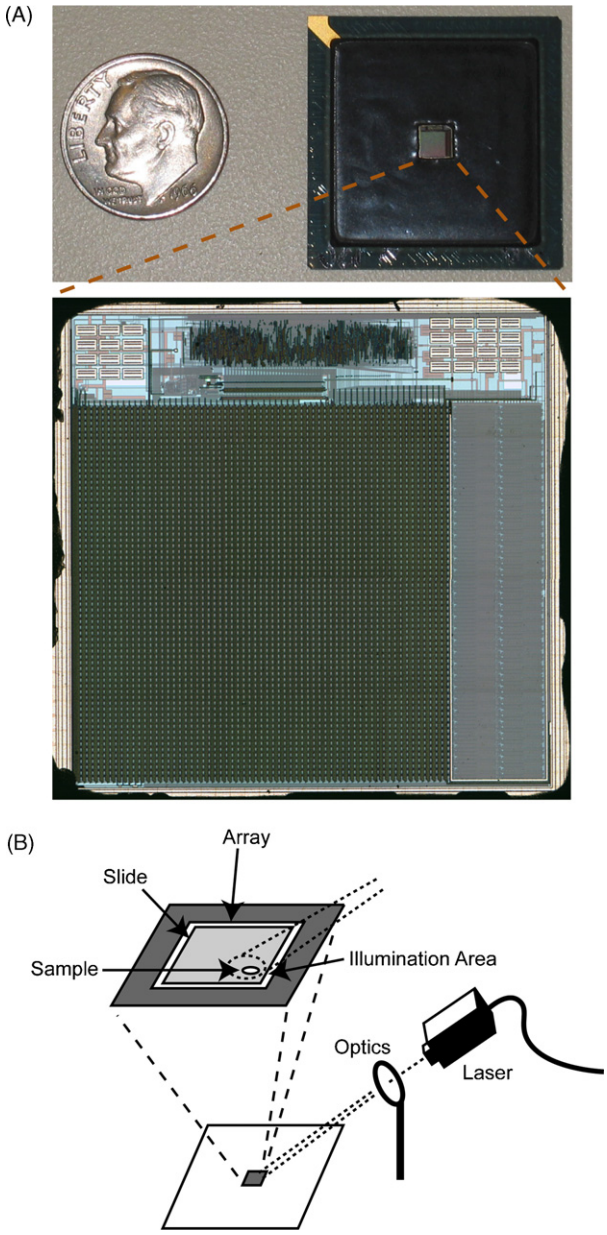

Fig. 1. (A) A photograph and microphotograph of the CMOS active microarray. The large square to the lower left is the 64-by-64 SPAD pixel array. The time-to-digital converters and supporting circuitry are at the top and right. The black border is the epoxy encapsulation. (B) A simplified diagram of the experimental setup.

much shorter than the lifetime of the measured dye, significant source background rejection results. Additional background rejection is effected through the use of a 22-layer TiO_2/SiO_2 thin-film interference filter deposited on the surface of the some of the arrays. The filter, prepared by ZC&R Coatings For Optics, Inc. (Torrance, CA, USA), has a long-wave-pass profile with a nominal cutoff wavelength of 500 nm, 30–40 dB rejection at the 406-nm source wavelength, and 92% transmission at the 655-nm emission wavelength of the quantum dots used in the microarray assay.

2.3. Quantum dots as donor fluorophores

Quantum dots, crystals of semiconductor a few nanometers in size, are an attractive donor-fluorophore choice for TR-FRET experiments. They have excellent photostability, allowing reliable and repeatable measurements with bright light sources. Their characteristic lifetimes are long, often in the 10–30 ns range as compared to several nanoseconds for typical organic dyes, reducing requirements on timing resolution. They are available in many colors, facilitating the optimization of detector sensitivity and quencher pairing. They also have broad excitation spectra, allowing for multi-probe experiments with a single light source and a simple optical path (Michalet et al., 2005).

The use of quantum dots for TR-FRET necessitates a modified assay protocol. In the simplest TR-FRET assays, the donor molecule is attached to the immobilized probe prior to hybridization. When quantum dots are employed as the donor fluorophores, however, we have found that nonspecific adsorption of quencher-labeled-target to the quantum dot complex causes extensive quenching independent of hybridization. To avoid this effect, we perform the hybridization step before the quantum dots have been attached to the probe, as shown in Fig. 2. First, probe molecules functionalized with biotin are immobilized on the substrate. Then, hybridization with quencher-modified analyte target is carried out. The quantum dots are introduced in the final step, in which they attach to the probe molecules through streptavidin–biotin binding.

2.4. Array calibration

The capability of the array for accurate lifetime measurement is demonstrated by measuring the lifetime of the pH-sensitive dye acridine in solutions with a range of pH values. Acridine, 98% (Fisher, Fair Lawn, NJ, USA) is dissolved in a 1 mM concentration in 0.1 M sodium phosphate buffers with pH values ranging from 5.4 to 7.6. Each solution is injected into an 80 μL chamber which is placed on top of the chip and illuminated from above. Although the excitation peak of acridine is at 380 nm, the 406-nm laser still generates a measurable emission. As the emission spectrum is broad and concentrated below 500 nm, an array chip with no excitation filter is used.

2.5. Oligonucleotide hybridization measurement

To demonstrate TR-FRET hybridization measurement using our sensor array, we measure the lifetime change in donor fluorophores bound to immobilized probe molecules as the concentration of quencher-modified-target is varied. We then repeat this experiment with fixed target concentration and varying probe density to observe the sensitivity of the TR-FRET signal to probe coverage variation.

We use streptavidin-conjugated Qdot 655 CdSe/ZnS quantum dots (Invitrogen, Carlsbad, CA, USA) as donors and QSY 21 (Invitrogen) as quenchers. All oligonucleotides are ordered fully modified from Operon (Huntsville, AL, USA) and used as received. The 20-mer probe molecules ($^{5'}$GTCAAGATGCTACCGTTCAG$^{3'}$) have an AminoC6 5′ modification for surface tethering and a BioTEG biotin 3′ modification to allow quantum dot attachment. Both 20-mer complementary ($^{5'}$CTGAACGGTAGCATCTTGAC$^{3'}$) and non-complementary ($^{5'}$GTCATGCCACCGAAGTATTG$^{3'}$) target molecules are 5′ modified with an AminoC6-linked QSY 21 quencher molecule.

A volume of 1 μL of probe solution is pipetted onto the *N*-hydroxysuccinimide (NHS) ester surface of a CodeLink Activated Slide (GE Healthcare, Chalfont St. Giles, UK) and maintained at 100% humidity and 25 °C for 3 h. After rinsing with deionized water, the substrate is immersed in a blocking solution (50 nM ethanolamine, 0.1 M Tris, adjusted with HCl to pH 9.0) at 50 °C for 1 h to deactivate remaining surface groups and rinsed again. The surface is then exposed to 5 μL target solution at 100% humidity and 25 °C for 4 h to enable hybridization. After rinsing with 4× SSC buffer, followed by immersion in 2× SSC (5 min, twice), 0.2× SSC (1 min), and 0.1×

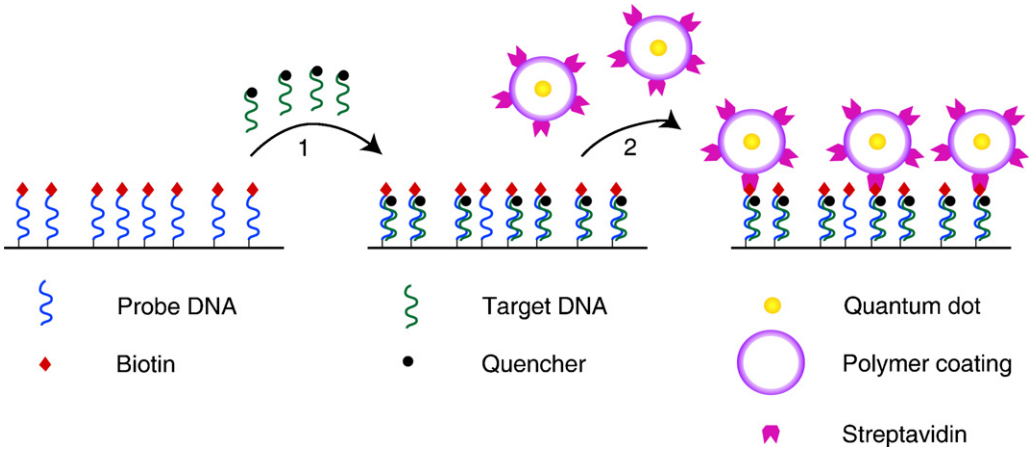

Fig. 2. A TR-FRET hybridization assay using quantum dot donors. The assay begins with biotinylated probe immobilized on the substrate. Then, (1), the probe is exposed to and allowed to hybridize with quencher-modified-target. Finally, (2), the probe-target complexes are treated with streptavidin-functionalized quantum dots, which attach to the biotin. If step (2) were performed first, the target would stick onto the surface of the quantum dot structures, quenching the quantum dots.

SSC (1 min), the surface is treated with 5 nM streptavidin Qdot 655 in 4× SSC for 1 h at 100% humidity and rinsed again with the same SSC sequence.

In the first hybridization experiment (the "target concentration series"), in which the probe concentration is fixed and the target concentration is varied, the probe solution consists of 120 μM probe in 0.5 M sodium phosphate buffer, pH 8.5, and the target solutions contain 0 nM, 20 nM, 40 nM, 80 nM, and 160 nM complementary and 160 nM non-complementary target in 4× SSC buffer, pH 7.0. In the second experiment (the "probe concentration series"), in which the probe concentration is varied and the target concentration is fixed, the probe solutions consist of 200 μM, 100 μM, 50 μM, and 25 μM in 1.0 M sodium phosphate buffer, pH 8.5, and the target solution contains 20 nM complementary target in 4× SSC, pH 7.0.

3. Results and discussion

3.1. TR-FRET quantum dot lifetime measurement

To find the quantum dot lifetime components, decay data are first deconvolved from the measured sensor impulse response function, as is standard in TCSPC measurements. Fig. 3a shows the sensor impulse response function as well as the measured decay profile of immobilized probe with attached streptavidin-conjugated Qdot 655 and no target. The impulse response, which represents the effect of the laser source on the measurement, is obtained using a configuration identical to that used in lifetime measurements (Fig. 1B), but with the sample omitted. It is shaped by a combination of deep-level traps and carrier diffusion effects (Cova et al., 1991; Ripamonti and Cova, 1985).

The deconvolved quantum dot lifetime data are fitted with biexponential decay functions, the longer of which is employed as the characteristic lifetime. Because of the complexity of quantum dots' band structure, their intensity decay profiles are generally not monoexponential and although a variety of models have been proposed, including stretched-exponential (Schlegel et al., 2002) decays, biexponential fits with associated longer and shorter lifetime components in the 15–35 ns and 1–5 ns ranges, respectively, are commonly used. While the physical origin of the two components is in dispute (Lee et al., 2005), they are generally agreed to be determined by distinct physical processes and, as such, are affected differently by FRET. For example, the shorter lifetime component has been hypothesized to depend on recombination events in the quantum dot core (Wang et al., 2003), which are less likely to be influenced by external FRET acceptors than surface state transitions. The longer lifetime is associated with a radiative decay rate and has a consistent value when the quantum dot is illuminated with a high-intensity source (Fisher et al., 2004). Unlike the shorter lifetime, it does not vary with temperature above 200 K (Lee et al., 2005).

In our measurements, we find the shorter lifetime component of the biexponential fit to be variable across identically prepared samples, with a standard deviation of as much as 87% of the mean. The longer component, on the other hand, is consistent, with a standard deviation limited to 4% of the mean, and is strongly correlated with the target concentration.

The average measured lifetime components for the probe-bound-quantum dots in Fig. 3a are 30.3 ns and 500 ps. These values have been verified with an independent measurement using standard TCSPC instrumentation consisting of an OB920 Fluorescence Lifetime Spectrometer (Edinburgh Instruments, Livingston, UK) and a Hamamatsu R928 PMT (Hamamatsu City, Japan). The lifetime components determined by that measurement are 30.4 ns and 605 ps.

3.2. Array calibration

Fig. 3b shows the results of the measurements of the lifetime of acridine as a function of pH compared with those in Ryder et al. (2001). The published data are measured using emission line-pass filters of 450 nm and 500 nm while our measurements represent averages over the emission spectrum. This accounts for our measured values falling between the published curves.

3.3. Target concentration series

A plot of the longer measured lifetimes for the full target sequence is shown in Fig. 4a. The error bars show the variation over three independent measurements and represent standard deviations in the range of 1–4% of the mean values. The measured lifetime can be seen to decrease monotonically with increasing target concentration over the range of concentrations tested. Furthermore, the measured lifetime when the probe is exposed to a high concentration (160 nM) of non-complementary target (TNC) is comparable to that measured when it is exposed to buffer containing no target (0 nM). This confirms that the measured lifetime change is the result of hybridization and not a non-sequence-specific effect.

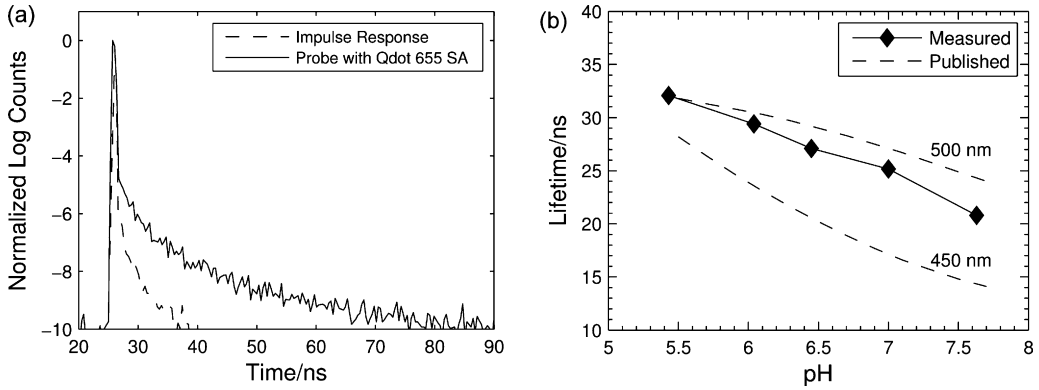

Fig. 3. (a) Semi-log plot of the measured sensor impulse response function as well as the fluorescence decay of Qdot-655-labeled probe with no hybridized target. (b) The measured lifetime of acridine in solutions with several pH values. The dashed curves represent acridine lifetime measurements reported in (Ryder et al., 2001) using 450 nm and 500 nm line-pass filters.

The lifetime reduction associated with FRET is a consequence of a non-radiative transfer of energy from the donor fluorophore to the quencher. The efficiency of this transfer depends on several factors including the overlap of the donor emission and quencher absorption spectra and the donor and quencher molecules' separation and relative orientation. In a given assay, the spectra are fixed and the relative orientations can be assumed to randomize and average (Clegg, 1992). The lifetime change, then, is primarily a function of molecular separation.

For a donor fluorophore with native lifetime τ_D, the quenched lifetime can be shown to be

$$\tau_{DQ} = \frac{\tau_D}{1 + (R_0/R)^6} \quad (1)$$

where R is the distance between the donor and quencher and R_0 is the Förster distance (Clegg, 1992), usually in the range of 10–100 Å (Periasamy, 2001). Because of the sixth-power dependence, FRET is only observable for molecular separations of less than several times R_0. In a TR-FRET expression assay, this criterion is only met in a statistically significant way upon hybridization. The fluorescent signal is a linear combination of the native and quenched decays (Vogel et al., 2006):

$$I(t) = A \exp\left(\frac{-t}{\tau_D}\right) + B \exp\left(\frac{-t}{\tau_{DQ}}\right). \quad (2)$$

As the intensities of the unquenched and quenched components, A and B, correspond to the relative number of unbound and bound probe molecules, the ratio of the quenched to total signal, $B/(A+B)$, determines F, the fractional occupancy of probe by bound target. Likewise, the average fluorescence lifetime, determined by the best monoexponential approximation to the fluorescence intensity decay, is proportional to F.

The large size of the quantum dot labels used as donors complicates this analysis. To enable their attachment to DNA, quantum dots, which themselves are only several nanometers across, are enclosed in a polymer shell which is then conjugated with streptavidin or another functional molecule, leading to a final structure that is 10–15 nm in diameter (Nisman et al., 2004). This limits the surface density of quantum dots to 5×10^{11} molecules/cm^2. If, as in our experiments, the surface probe coverage is greater than this, there may be more than one probe molecule per quantum dot, adding complexity to the quenching dynamics as some quencher-modified target molecules may hybridize to probe molecules with no associated quantum dot donor. These target molecules will induce a reduced quenching effect that depends on their distance from the nearest probe-bound-quantum dots according to Eq. (1). Nevertheless, except in assays utilizing few enough analyte molecules to invalidate ensemble averaging, the overall mean lifetime will still be proportional to the fractional occupancy. This is validated in Fig. 4b, which shows an almost linear relationship between the measured longer lifetime component and the estimated fractional occupancy, F.

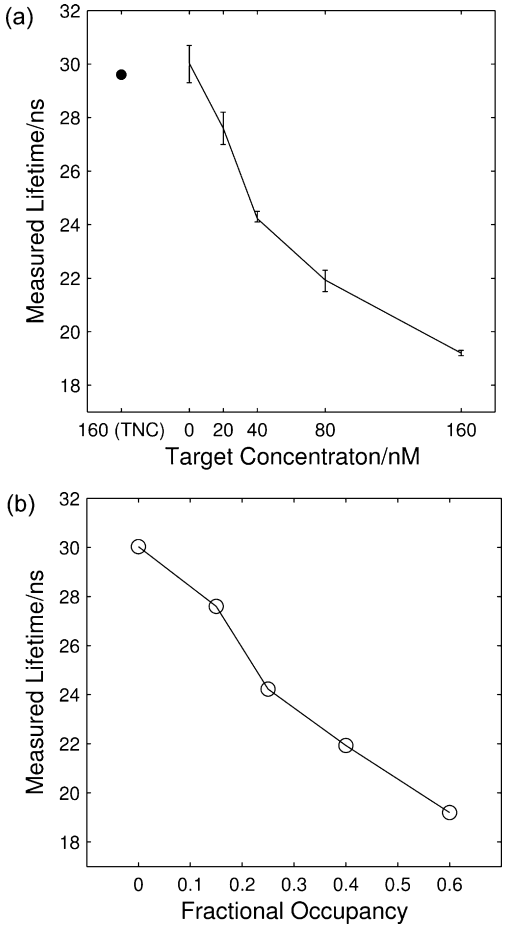

Fig. 4. (a) Measured longer lifetime component after hybridization with complementary target solutions of several concentrations as well as with 160 nM non-complementary target. Error bars are based on three independent measurements. (b) The measured lifetime as a function of estimated fractional occupancy (F).

In the context of TR-FRET assays, the size of the quantum dot structure also increases the minimum possible separation between the quantum dot donor and an associated quencher molecule. However, this is compensated by the quantum dots' high quantum yield, which leads to a larger Förster radius according to the relationship $R^6 = A\Phi$, where Φ is the donor quantum yield and A is a constant depending on the spectral overlap of the donor emission and quencher absorption and the refractive index of the medium between them (Förster, 1948; Clapp et al., 2004). For example, with the Qdot-655 donor and QSY-21 quencher used in our experiments, we calculate $R_0 \approx 70$ Å. This is comparable to the expected maximum separation of the donor and quencher upon hybridization, determined by the sum of the quantum dot radius (50–75 Å), the double-helix diameter (~20 Å), and the lengths of linkers used (<20 Å). Consequently, even in the worst case, hybridization brings the quencher within twice the Förster radius of the quantum dot donor, inducing a measurable FRET interaction as is evident in Fig. 4.

3.4. TR-FRET signal dependence on target and probe concentrations

One feature of TR-FRET that distinguishes it from conventional assays is the dependence of the signal (in this case, the average fluorescence lifetime) on F, the fraction of bound probe molecules, rather than on their absolute number. As a consequence, for low probe densities, TR-FRET has greater immunity to variations in probe surface coverage than standard microarray platforms. To quantify this, we can apply the analysis of fractional occupancy developed by Ekins and Chu (1991) for immunoassays to DNA. Let K be the hybridization equilibrium constant,

$$K = \frac{[PT]}{([P]-[PT])([T]-[PT])} \tag{3}$$

where $[P]$ and $[T]$ are, respectively, the probe and target concentrations and $[PT]$ is the concentration of bound probe-target pairs, all measured in solution during hybridization. Then the fractional occupancy

$$F = \frac{[PT]}{[P]} \tag{4}$$

can be found by solving

$$F^2 - (1/[\hat{P}] + [\hat{T}]/[\hat{P}] + 1)F + [\hat{T}]/[\hat{P}] = 0 \tag{5}$$

where $[\hat{P}] = K[P]$ and $[\hat{T}] = K[T]$. The bound probe concentration, C_{PT}, normalized by K^{-1} is given by

$$C_{PT} = K[PT] = [\hat{P}]F. \tag{6}$$

Fig. 5a shows contour plots of the fractional occupancy, F, and bound probe concentration, C_{PT}, as functions of $[\hat{P}]$ and $[\hat{T}]$. For low probe densities, F becomes independent of probe concentration, varying less than 1% for $[\hat{P}] < 0.01$. In this region, measurable target concentrations (where F varies significantly with $[T]$) range approximately from $0.1K^{-1}$ to $10K^{-1}$. When $[P] > K^{-1}$, measurable target concentrations depend more strongly on $[P]$ than on K and range approximately from $0.1[P]$ to $10[P]$. On the other hand, C_{PT}, which corresponds to the signal measured in standard microarray assays, varies greatly with probe coverage but changes little with target concentration for the medium to low probe density range of $[\hat{P}] < 1$.

The equilibrium constant, K, upon which F and C_{PT} depend, is sensitive to many factors including temperature, ionic strength, and probe length, and is consequently difficult to quantify. It is generally observed (Levkicky and Horgan, 2005), however, to fall between $10^7\ M^{-1}$ and $10^9\ M^{-1}$ for surface-based assays. Assuming a typical probe surface density of 10^{12}–10^{13} probes/cm^2 (Levkicky and Horgan, 2005), a spot diameter of 100 μm and a hybridization volume of 100 μL, we find $[\hat{P}] < 1.5 \times 10^{-2}$. In this situation, F varies less than 2% with variation in $[P]$ up to 10%, and the measurable target concentration falls in the range 0.1 nM < $[T]$ <1 μM. This range can be modified by varying the hybridization conditions to adjust the value of K.

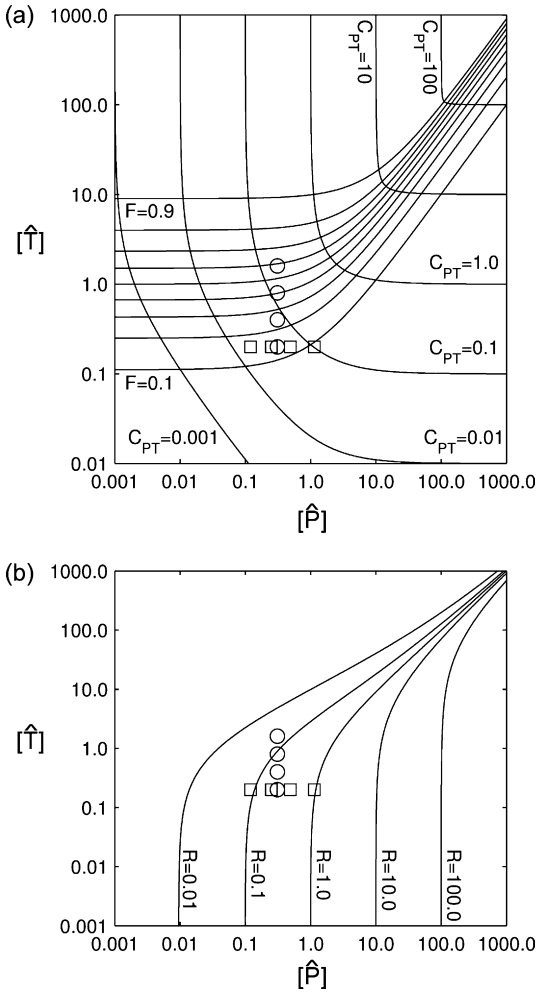

Fig. 5. Contour plots of (a) fractional occupancy (F) and normalized bound probe concentration (C_{PT}) and (b) the ratio (R) of sensitivity with respect to probe density of F to C_{PT}, as functions of probe and target concentration in hybridization solution. In plot (b), the $R = 1.0$ curve represents the boundary between the regions where F varies less than C_{PT} (above and left) and more than C_{PT} (below and right). The circles represent the estimated experimental points in the target concentration series. The squares represent the estimated experimental points in the probe concentration series.

Based on previous studies (Levkicky and Horgan, 2005; Gong et al., 2006; Peterson et al., 2002), the equilibrium constant, K, for our experiments is assumed to be approximately $1 \times 10^7\ M^{-1}$ and the surface density of probe for the target concentration series is approximately 1.9×10^{12} molecules/cm^2. Probe surface densities are extrapolated from (Gong et al., 2006), in which probe immobilization is carried out under similar conditions and accurately measured with ^{32}P radiometric quantification. From our spot size of 0.05 cm^2, we can calculate $[\hat{P}] \approx 0.31$. We therefore expect F to vary with $[T]$ for 10 nM < $[T]$ < 1 μM. While the probe density in the target concentration series is higher than the maximum quantum dot surface density, we expect the dependence of F on $[T]$ to remain monotonic. The measured lifetime values shown in Fig. 4 corroborate these predictions.

Fig. 6 shows the longer lifetime components of a fixed 20 nM concentration of target hybridized onto surfaces with several different probe densities. The error bars are based on three independent measurements. The probe concentrations of 25 μM, 50 μM, 100 μM, and 200 μM in 1 M buffer give probe surface densities of approximately 7.5×10^{11}, 1.5×10^{12}, 3.0×10^{12}, and 7.0×10^{12} molecules/cm^2, corresponding to values of $[\hat{P}]$ of 0.12, 0.25, 0.49, and 1.14, respectively. It should be noted that for saturating target concentrations, the equilibrium constant, K, has been shown to decrease for probe concentrations higher than 4.0×10^{12} molecules/cm^2 (Steel et al., 1998). The relatively low target concentration employed in this experiment may mitigate that effect somewhat. However, the estimated value of $[\hat{P}]$ for the probe density of 7.0×10^{12} molecules/cm^2 might be slightly low. As $[\hat{T}] \approx 0.2$, with the above range of values of $[\hat{P}]$, we expect to see a decrease in F with probe density, resulting in a longer average lifetime. As can be seen in Fig. 6, the lifetime does increase slightly, while remaining nearly constant.

Finally, we can compare the sensitivities of F and C_{PT} to variations in probe coverage by taking the ratio of their sensitivities with respect to $[\hat{P}]$. Defining

$$V_F = \frac{1}{F}\frac{\partial F}{\partial[\hat{P}]} \tag{7}$$

and

$$V_B = \frac{1}{C_{PT}}\frac{\partial C_{PT}}{\partial[\hat{P}]}, \tag{8}$$

Fig. 5b shows a contour plot of $R = V_F/V_B$ as a function of $[\hat{P}]$ and $[\hat{T}]$. When $[\hat{P}] < 1$ or when $[\hat{P}] < [\hat{T}]$, $R < 1$, indicating that there is less variation in fractional occupancy than in bound probe concentration. For $[\hat{P}] > [\hat{T}]$ and $[\hat{P}] > 1$, however, most available target is bound and increasing the probe density reduces F without binding additional target. For low probe densities, then, nonuniformities in probe coverage due to solution or surface inhomogeneity, spotting volume variation, and other experimental factors will have less of an effect on the reliability of TR-FRET than conventional assays.

3.5. System sensitivity and dynamic range

With the system as described and tested, bulk target concentrations as low as 20 nM, corresponding to 0.1 pmol of target in the 5 μL hybridization solution volume, have been measured and the verified dynamic range is 20–160 nM. As can be seen in Fig. 5a, this can theoretically be extended to two orders of magnitude through optimization of the choice of donor–quencher pair. Furthermore, as the dynamic range is dependent on the equilibrium constant, K, varying the probe surface density and hybridization conditions can allow the same system to measure different ranges of target concentration. For example, with $K = 10^9\ M^{-1}$, using the same 5 μL volume, 0.5 fmol of target corresponds to $F = 0.1$ and is within the theoretical range of detection. Investigations of these optimizations will be carried out in future work.

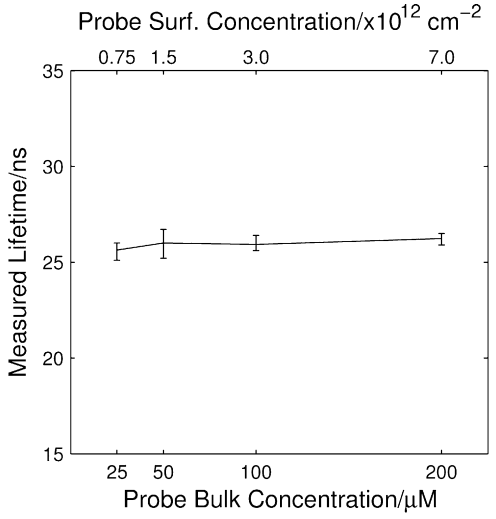

Fig. 6. Measured longer lifetime component after hybridization with 20 nM complementary target as a function of probe surface density. Error bars are based on three independent measurements.

4. Conclusions

We have demonstrated the use of a novel active sensor array for TR-FRET-based oligonucleotide microarray analysis. The array is capable of determining the concentration of quencher-modified-target molecules complementary to immobilized probe labeled with fluorescent quantum dot tags. We have discussed several potential advantages of this system over conventional microarray technologies, including reduced dependence on probe surface coverage. FRET-based time-resolved fluorescence techniques can be applied to any affinity-based assay.

Acknowledgments

This work was made possible by funding from the National Institutes of Health under grants HG003089 and ES016074, the National Science Foundation under grant 0428544, and the New York State Office of Science, Technology, and Academic Research (NYSTAR). The authors would also like to acknowledge Edoardo Charbon of EPFL, Lausanne, Switzerland, for his contributions to the design of the CMOS array and Steffen Jockusch for his kind assistance with the PMT measurements.

References

Auburn, R.P., Kreil, D.P., Meadows, L.A., Fischer, B., Matilla, S.S., Russell, S., 2005. Trends in Biotechnology 23 (7), 374–379.
Becker, W., Bergmann, A., Hink, M.A., König, K., Benndorf, K., Biskup, C., 2004. Microscopy Research and Technique 63, 58–66.
Cardullo, R.A., Agrawal, S., Flores, C., Zamecnik, P.C., Wolf, D.E., 1988. Proceedings of the National Academy of Sciences of the United States of America 85 (23), 8790–8794.
Chittur, S.V., 2004. Combinatorial Chemistry and High Throughput Screening 7 (6), 531–537.
Clapp, A.R., Medintz, I.L., Mauro, J.M., Fisher, B.R., Bawendi, M.G., 2004. Journal of the American Chemical Society 126, 301–310.
Clegg, R., 1992. Methods Enzymology 211, 353–388.
Cova, S., Lacaita, A., Ripamonti, G., 1991. IEEE Electron Device Letters 12 (12), 685–687.
De Grauw, C.J., Gerristen, H.C., 2001. Applied Spectroscopy 55 (6), 670–678.
Divne, A.M., Allen, M., 2005. Forensic Science International 154 (2–3), 111–121.
Dowling, K., Hyde, S.C.W., Dainty, J.C., French, P.M.W., Hares, J.D., 1997. Optics Communications 135 (1–3), 27–31.
Draghici, S., Khatri, P., Eklund, A.C., Szallasi, Z., 2006. Trends in Genetics 22 (2), 101–109.
Ekins, R.P., Chu, F.W., 1991. Clinical Chemistry 37 (11), 1955–1967.
Fisher, B.R., Eisler, H.-J., Stott, N.E., Bawendi, M.G., 2004. Journal of Physical Chemistry B 108 (1), 143–148.
Forrest, M.S., Lan, Q., Hubbard, A.E., Zhang, L., Vermeulen, R., Zhao, X., Li, G., Wu, Y.Y., Shen, M., Yin, S., Chanock, S.J., Rothman, N., Smith, M.T., 2005. Environmental Health Perspectives 113 (6), 801–807.
Förster, T., 1948. Annalen der Physik 2, 55–75.
Gong, P., Harbers, G.M., Grainger, D.W., 2006. Analytical Chemistry 78 (7), 2342–2351.
Harris, C.M., Selinger, B.K., 1979. Australian Journal of Chemistry 32, 2111–2129.
Heller, M.J., 2002. Annual Review of Biomedical Engineering 4, 129–153.
Hoheisel, J.D., 2006. Nature Reviews Genetics 7 (3), 200–210.
Kawasaki, E.S., 2006. Journal of Biomolecular Techniques 17 (3), 200–206.
Lamture, J.B., Beattie, K.L., Burke, B.E., Eggers, M.D., Ehrlich, D.J., Fowler, R., Hollis, M.A., Kosicki, B.B., Reich, R.K., Smith, S.R., 1994. Nucleic Acids Research 22 (11), 2121–2125.

Lee, W.Z., Shu, G.W., Wang, J.S., Shen, J.L., Lin, C.A., Chang, W.H., Ruan, R.C., Chou, W.C., Lu, C.H., Lee, Y.C., 2005. Nanotechnology 16 (9), 1517–1521.
Levkicky, R., Horgan, A., 2005. Trends in Biotechnology 23 (3), 143–149.
Mallard, F., Marchand, G., Ginot, F., Camagnolo, R., 2005. Biosensors and Bioelectronics 20 (9), 1813–1820.
Mary-Huard, T., Daudin, J.J., Robin, S., Bitton, F., Cabannes, E., Hilson, P., 2004. BMC Bioinformatics 5 (1), 63.
Michalet, X., Pinaud, F.F., Bentolila, L.A., Tsay, J.M., Doose, S., Li, J.J., Sundaresan, G., Wu, A.M., Gambhir, S.S., Weiss, S., 2005. Science 307 (5709), 538–544.
Motamed-Khorasani, A., Jurisica, I., Letarte, M., Shar, P.A., Parkes, R.K., Zhang, X., Evangelou, A., Rosen, B., Murphy, K.J., Brown, T.J., 2007. Oncogene 26, 198–214.
Murphy Jr., G.M., 2006. Journal of Psychopharmacology 20 (Suppl. 4), 72–78.
Nicholas, S.Y.B.M.L., Barry, P., 2006. Nephron Experimental Nephrology 103, e41–e49.
Nisman, R., Dellaire, G., Ren, Y., Li, R., Bazett-Jones, D.P., 2004. Journal of Histochemistry and Cytochemistry 52 (1), 13–18.
Peeters, J.K., Van der Spek, P.J., 2005. Cell Biochemistry and Biophysics 43 (1), 149–166.
Periasamy, A., 2001. Journal of Biomedical Optics 6 (3), 287–291.
Peterson, A.W., Wolf, L.K., Georgiadis, R.M., 2002. Journal of the American Chemical Society 124, 14601–14607.
Ramakrishnan, R., Dorris, D., Lublinsky, A., Nguyen, A., Domanus, M., Prokhorova, A., Gieser, L., Touman, E., Lockner, R., Tata, M., Zhu, X., Patterson, M., Shippy, R., Sendera, T.J., Mazumder, A., 2002. Nucleic Acids Research 30 (7), e30.
Ripamonti, G., Cova, S., 1985. Solid-State Electronics 28 (9), 925–931.
Rochas, A., Pauchard, A.R., Besse, P.-A., Pantic, D., Prijic, Z., Popovic, R.S., 2002. IEEE Transactions on Electron Devices 49 (3), 387–394.
Ryder, A.D., Power, S., Glynn, T.J., Morrison, J.J., 2001. Proceedings of SPIE 4259, 102–109.
Schlegel, G., Bohnenberger, J., Poapova, I., Mews, A., 2002. Physical Review Letters 88 (13), 137401.
Schroers, R., Griesinger, F., Trümper, L., Haase, D., Kulle, B., Klein-Hitpass, L., Sellmann, L., Dührsen, U., Dürig, J., 2005. Leukemia 19, 750–758.
Schwartz, D.E., Charbon, E., Shepard, K.L., 2007. 2007 IEEE Symposium on VLSI Circuits, pp. 144–145.
Sharman, K.K., Periasamy, A., Ashworth, H., Demas, J.N., Snow, N.H., 1999. Analytical Chemistry 71 (5), 947–952.
Song, Y., Dai, E., Wang, J., Liu, H., Zhai, J., Chen, C., Du, Z., Guo, Z., Yang, R., 2006. Molecular and Cellular Probes 20 (2), 121–127.
Steel, A.B., Herne, T.M., Tarlov, M.J., 1998. Analytical Chemistry 70 (22), 4670–4677.
Vo-Dinh, T., Alarie, J.P., Isola, N., Landis, D., Wintenberg, A.L., Ericson, M.N., 1999. Analytical Chemistry 71 (2), 358–363.
Vogel, S.S., Thaler, C., Srinagesh, V.K., 2006. Science's STKE 331, re2.
Wang, X.F., Uchida, T., Coleman, D.M., Minami, S., 1991. Applied Spectroscopy 45 (3), 360–366.
Wang, X., Qu, L., Zhang, J., Peng, X., Xiao, M., 2003. Nano Letters 3 (8), 1103–1106.
Watters, J.W., McLeod, H.L., 2003. Biochimica et Biophysica Acta 1603 (2), 99–111.
Wilson, W.J., Stout, C.L., DeSantis, T.Z., Stilwell, J.L., Carrano, A.V., Andersen, G.L., 2002. Molecular and Cellular Probes 16 (2), 119–127.